High Performance Thin-Film Composite Forward Osmosis Membrane

ARTICLE *in* ENVIRONMENTAL SCIENCE AND TECHNOLOGY · MAY 2010

Impact Factor: 5.33 · DOI: 10.1021/es1002555 · Source: PubMed

Environ. Sci. Technol. **2010,** *44,* 3812–3818

High Performance Thin-Film Composite Forward Osmosis Membrane

NGAI YIN YIP, ALBERTO TIRAFERRI, WILLIAM A. PHILLIP, JESSICA D. SCHIFFMAN, AND MENACHEM ELIMELECH*

Department of Chemical Engineering, Environmental Engineering Program, Yale University, New Haven, Connecticut 06520-8286

Received January 24, 2010. Revised manuscript received April 5, 2010. Accepted April 6, 2010.

Recent studies show that osmotically driven membrane processes may be a viable technology for desalination, water and wastewater treatment, and power generation. However, the absence of a membrane designed for such processes is a significant obstacle hindering further advancements of this technology. This work presents the development of a high performance thin-film composite membrane for forward osmosis applications. The membrane consists of a selective polyamide active layer formed by interfacial polymerization on top of a polysulfone support layer fabricated by phase separation onto a thin (40 μm) polyester nonwoven fabric. By careful selection of the polysulfone casting solution (i.e., polymer concentration and solvent composition) and tailoring the casting process, we produced a support layer with a mix of finger-like and sponge-like morphologies that give significantly enhanced membrane performance. The structure and performance of the new thin-film composite forward osmosis membrane are compared with those of commercial membranes. Using a 1.5 M NaCl draw solution and a pure water feed, the fabricated membranes produced water fluxes exceeding 18 L $m^{-2}h^{-1}$, while consistently maintaining observed salt rejection greater than 97%. The high water flux of the fabricated thin-film composite forward osmosis membranes was directly related to the thickness, porosity, tortuosity, and pore structure of the polysulfone support layer. Furthermore, membrane performance did not degrade after prolonged exposure to an ammonium bicarbonate draw solution.

Introduction

Osmotically driven membrane processes have the potential to sustainably produce clean drinking water or electric power. These membrane-based technologies exploit the natural phenomenon of osmosis, which occurs when two solutions of differing concentration are placed on opposite sides of a semipermeable membrane. The generated osmotic pressure difference drives the permeation of water across the membrane from the dilute solution to the concentrated solution, while the selective property of the membrane retains the solutes in their respective solutions. Engineered osmosis relies on the appropriate selection of the concentrated draw solution. More energy efficient processes can be realized when the separation of draw solute from water requires less energy than the separation of water from contaminants dissolved in the dilute feed solution.

Forward osmosis (FO) is a subset of osmotically driven membrane processes, which has promising applications in seawater desalination (*1, 2*), wastewater reclamation (*3*−*5*), industrial wastewater treatment (*2, 6*), osmotic membrane bioreactors (*7*), and liquid food processing (*2, 8, 9*). For example, in a novel FO desalination process, a concentrated draw solution of ammonia-carbon dioxide is used to draw water from a saline feed solution. The diluted draw solution is then fed to a distillation column where low-grade heat is used to remove the dissolved gases, thus producing fresh water (*10*).

Despite the potential to address key issues surrounding global water and energy demands, osmotically driven membrane processes have yet to progress significantly beyond conceptualization. The major obstacle to advancing this technology is the lack of an adequate membrane. A membrane designed for an osmotically driven process should reject dissolved solutes, produce high permeate water fluxes, be compatible with the selected draw solution, and withstand the mechanical stresses generated by the operating conditions. Existing commercial membranes lack one or more of the above-mentioned characteristics, inhibiting their use in osmotically driven membrane processes. Commercial FO membranes are made from cellulose triacetate (CTA) which degrades when exposed to an ammonium bicarbonate draw solution (*11*). Additionally, cellulose acetate membranes have relatively low pure water permeability and salt rejection, which limits their use for desalination. Alternatively, conventional thin-film composite (TFC) reverse osmosis (RO) membranes exhibit high salt rejection and satisfy the chemical stability and mechanical strength requirements. However, TFC membranes yield very poor permeate water fluxes in FO because they are designed for pressure-driven membrane processes, such as RO (*12*).

TFC-RO membranes fail in FO operation because the thick and dense support layers, necessary to withstand large hydraulic pressures, result in internal concentration polarization (ICP). ICP adversely affects the performance of all asymmetric membranes in FO, with the effects being exacerbated for TFC-RO membranes due to their thick and dense porous support. The porous support layer acts as a diffusive boundary layer, which severely reduces the osmotic pressure difference across the active layer (*13*). Because this boundary layer is unperturbed by stirring (*13, 14*), modifying the support layers is essential to minimize the performance-limiting effects of ICP that currently hinder TFC membranes (*10*). Prior studies have demonstrated, through both experiments and modeling, that the additional resistance to mass transfer of this boundary layer is proportional to the support layer thickness and tortuosity, and inversely proportional to the support layer porosity (*14*−*16*). Therefore, the ideal support layers for FO membranes to enhance performance would be very thin, highly porous, and provide a direct path from the draw solution to the active surface of the membrane.

In this work, we demonstrate the fabrication of a TFC membrane tailored for FO operation. Innovative modifications made to the membrane casting procedure, as well as the resultant effects of these changes on the microstructure of the membranes are described. Salt rejection and water flux of the newly fabricated TFC-FO membranes are compared to commercially available RO and FO membranes. These performance results are linked to the membrane

* Corresponding author phone: (203) 432-2789; e-mail: menachem.elimelech@yale.edu.

10.1021/es1002555
Published on Web 04/21/2010

structural properties. Finally, the chemical stability of the TFC-FO membrane in a concentrated ammonium bicarbonate solution is demonstrated, indicating potential application in the ammonia-carbon dioxide FO process. This work aims to demonstrate the ability to fabricate membranes with a structure adapted to FO processes, thus providing a basis for further developments of osmotically driven membranes.

Materials and Methods

Materials and Chemicals. Polysulfone (PSf) beads (M_n: 22,000 Da), 1-methyl-2-pyrrolidinone (NMP, anhydrous, 99.5%), *N*,*N*-dimethylformamide (DMF, anhydrous, 99.8%), 1,3-phenylenediamine (MPD, >99%), and 1,3,5-benzenetricarbonyl trichloride (TMC, 98%) were used as received (Sigma-Aldrich, St. Louis, MO). TMC was dispersed in Isopar-G, a proprietary nonpolar organic solvent (Univar, Redmond, WA). For the membrane performance tests, sodium chloride (NaCl, crystals, ACS reagent) from J.T. Baker (Phillipsburg, NJ) and ammonium bicarbonate (NH_4HCO_3, powder, certified ACS) from Fisher Scientific (Pittsburgh, PA) were dissolved in deionized water (DI) obtained from a Milli-Q ultrapure water purification system (Millipore, Billerica, MA).

A commercial polyester nonwoven fabric (PET, grade 3249, Ahlstrom, Helsinki, Finland) was used as a backing layer for the PSf supports. The thin (40 μm) PET fabric had a relatively open structure. Commercial asymmetric cellulose triacetate (HTI-CTA) forward osmosis membranes (Hydration Technology Inc., Albany, OR) and thin-film composite seawater reverse osmosis membranes (TFC-RO, SW30-HR, Dow Chemical Company, Midland, MI) were acquired for comparison. Additionally, the PET fabric layer of some TFC-RO samples was removed according to procedures described in our previous study (*12*); these membrane samples are designated as "TFC-RO No PET".

Casting of Polysulfone Support. PSf beads (12 wt %) were dissolved in a mixed solvent system of DMF and NMP, at a ratio of 1:3 DMF:NMP on a weight basis. The solution was stirred at room temperature (23 °C) for 8 h and then stored in a desiccator for at least 15 h prior to casting. The thin, low-density PET fabric was attached to a clean glass plate using laboratory adhesive tape. NMP was applied to wet the fabric and the excess NMP was removed using an air knife. A casting knife (Gardco, Pompano Beach, FL), set at a gate height of 150 μm, was used to spread the PSf solution onto the wetted PET fabric. The whole composite was immediately immersed in a precipitation bath containing 3 wt % NMP in DI at room temperature to initiate the phase separation. The support membrane was allowed to sit in the precipitation bath for 10 min, at which point it was transferred to a DI bath for storage until polyamide formation.

Interfacial Polymerization of TFC Membrane. Polyamide TFC membranes were produced by first immersing a hand-cast PSf support membrane in an aqueous solution of 3.4 wt % MPD for 120 s. An air knife was then used to remove the excess MPD solution from the membrane surface. Next, the MPD-saturated support membrane was immersed into the 0.15 wt % TMC in ISOPAR-G solution for 60 s, resulting in the formation of an ultrathin polyamide film. The composite membranes were cured in DI at 95 °C for 120 s, then rinsed with a 200 ppm NaOCl aqueous solution for 120 s, followed by rinsing for 30 s with a 1000 ppm $NaHSO_3$ aqueous solution, before a final heat curing step at 95 °C for 120 s. The fabricated TFC membranes (TFC-FO) were rinsed thoroughly and stored in DI at 4 °C. This formulation was adapted from a patent for interfacial polymerization of polyamide active layer on PSf support for TFC-RO membranes (*17*).

SEM Imaging and Thickness Measurement of Membrane. Micrographs of the membranes were obtained utilizing a Hitachi Ultra-High-Resolution Analytical Field Emission Scanning Electron Microscope (FE-SEM) SU-70. Cross sections were obtained by flash-freezing the membranes using liquid nitrogen, then cracking the sample. An Emitech SC7620 sputtering machine was used to coat all samples for 15−30 s with gold−platinum. The thickness of the membranes was measured using a digital micrometer (series 293−330, Mitutoyo, Mississauga, Ontario Canada) at 5 different locations for each membrane sample.

Testing Membrane Performance in FO Mode. The experimental crossflow FO system employed is similar to that described in our previous studies (*10, 12, 13*). The unit was custom built with channel dimensions of 77 mm long, 26 mm wide, and 3 mm deep on both sides of the membrane. We operated the unit with cocurrent cross-flows without mesh spacers. The volume of both feed and draw solutions was 2.0 L at the start of each experimental run. Variable speed gear pumps (Cole-Parmer, Vernon Hills, IL) were used to pump the solutions in closed loops at 1.0 L/min (21.4 cm/s crossflow velocity) and a water bath (Neslab, Newington, NH) maintained the temperature of both the feed and draw solutions at 25 ± 0.5 °C. All membranes were tested in FO mode, with the porous support layer against the draw solution and the active layer against the feed solution.

The experimental protocol to determine water flux is similar to that previously described (*10, 18*). A 1.5 M NaCl solution was used for the draw solution and DI was used as the feed solution. The resulting bulk osmotic pressure difference, $\Delta\pi$, was 1111 psi (75.6 atm), calculated by a software package from OLI Systems, Inc. (Morris Plains, NJ). After the water flux and temperature stabilized, the flux was taken as the average reading over 1 h. The draw solution concentration is assumed to be constant throughout the experiment, since the volumetric water flux was low relative to the volume of draw solution.

A similar experimental protocol was used to determine membrane performance and chemical stability with an ammonium bicarbonate draw solution (1.5 M NH_4HCO_3). After the initial test, the membrane was stored in 1.5 M NH_4HCO_3 (pH 7.9) at 4 °C for 7 days, removed from the bath, and retested. The bath was used to simulate prolonged exposure to high concentrations of NH_4HCO_3. Storage at low temperature minimized potential growth of microorganisms on the membrane.

Determination of Pure Water Permeability and Salt Rejection. Pure water permeability and salt rejection of the TFC-FO and commercial membranes were evaluated in a laboratory-scale crossflow RO test unit (*19*). The effective membrane area was 20.02 cm^2, the crossflow velocity was fixed at 21.4 cm/s, and the temperature was constant at 25 ± 0.5 °C. The loaded membrane was first compacted with DI at an applied pressure, ΔP, of 400 psi (27.2 atm) until the permeate flux reached a steady state (at least 15 h). Pure water flux, J_w, was calculated by dividing the volumetric permeate rate by the membrane area. Salt rejection was characterized by keeping the applied pressure at 400 psi (27.2 atm) and measuring rejection of 50 mM NaCl solution using a calibrated conductivity meter (Oakton Instruments, Vernon Hills, IL).

Intrinsic water permeability, A, was determined by dividing the water flux by the applied pressure, $A = J_w/\Delta P$. Observed NaCl rejection, R, was determined from the difference in bulk feed (c_b) and permeate (c_p) salt concentrations, $R = 1 - c_p/c_b$. The rejection values for each sample are the average of three different measurements collected over ~30 min each. The solute permeability coefficient, B, was determined from (*11, 20*):

$$B = J_w\left(\frac{1-R}{R}\right)\exp\left(-\frac{J_w}{k}\right) \quad (1)$$

where k, the crossflow cell mass transfer coefficient, is calculated from correlations for this geometry (*21*).

Determination of FO Membrane Structural Parameters. The support layer resistance to solute diffusion, K, of one TFC-FO membrane was determined using the experimental protocol previously described (*13*). Water flux was measured in FO mode with DI as the feed solution and NaCl draw concentrations of 0.05, 0.1, 0.5, 1.0, and 1.5 M. The resulting flux versus osmotic pressure data was used to calculate the resistance to solute diffusion, K, via fitting to the following (*15*):

$$K = \left(\frac{1}{J_w}\right)\ln\frac{B + A\pi_{D,b}}{B + J_w + A\pi_{F,m}} \quad (2)$$

where J_w is the measured water flux, $\pi_{D,b}$ the bulk osmotic pressure of the draw solution, and $\pi_{F,m}$ the osmotic pressure at the membrane surface on the feed side (0 atm for DI feed). The resistance to diffusion K can be expressed as the reciprocal of a thin film mass transfer coefficient (*14*):

$$K = \frac{t_s\tau}{D\varepsilon} \quad (3)$$

where D is the diffusion coefficient of the draw solute, t_s is the support layer thickness, τ the tortuosity, and ε the porosity (*13*). We define the membrane structural parameter S:

$$S = KD = \frac{t_s\tau}{\varepsilon} \quad (4)$$

which is independent of the draw solution properties, assuming the draw solutes do not swell or plasticize the PSf and PET layers.

Results and Discussion

Membrane Microstructure and Morphology. The active surface of the TFC-FO membrane has a uniform ridge-and-valley morphology (Figures 1a and S1 of the Supporting Information), which is characteristic of polyamide membranes formed using an interfacial polymerization (*22*). The polyamide layer appears continuous, with high salt rejections observed in RO tests, thereby indicating that a functional selective layer was formed. After carefully removing the PET nonwoven fabric, the bottom surface of the PSf support layer was imaged, and the distinct, highly porous structure of this surface is shown in Figures 1b and S2 of the Supporting Information. Pore diameters on the bottom surface of the PSf support layer range from 2 to 10 μm; similar values of 5 to 12 μm are obtained from the cross-sectional SEM micrographs shown in Figures 2a and S3 of the Supporting Information. The average thickness of the membranes as measured by micrometer is 95.9 $\pm$ 12.6 μm. A finger-like morphology spans most of the PSf layer thickness, but the higher magnification micrograph in Figure 2b reveals a thin, 1- to 2-μm layer consisting of a dense sponge-like morphology near the top surface. This sponge-like morphology is favorable for the formation of an integral polyamide layer (*11*). No change in morphology of the membrane was observed after pressurization in RO experiments.

Producing a PSf support membrane with a thin layer of the sponge-like morphology on top of a finger-like layer is critical to fabricating a robust TFC-FO membrane. The sponge-like layer allows for an integral PA layer to form while the finger-like layer decreases the resistance to mass transfer. This finding is consistent with previous reports on TFC membranes; membranes with a dense support layer were better able to reject dissolved salts, but were hindered by low water fluxes (*23*).

The use of a mixed solvent system facilitated the formation of the desired microstructure. Immersing the cast thin film of polymer solution into the nonsolvent (water) bath results in the nonsolvent permeating into the polymer solution. Along with this in-flux of nonsolvent into the polymer solution, there is also an out-flux of solvent from the polymer

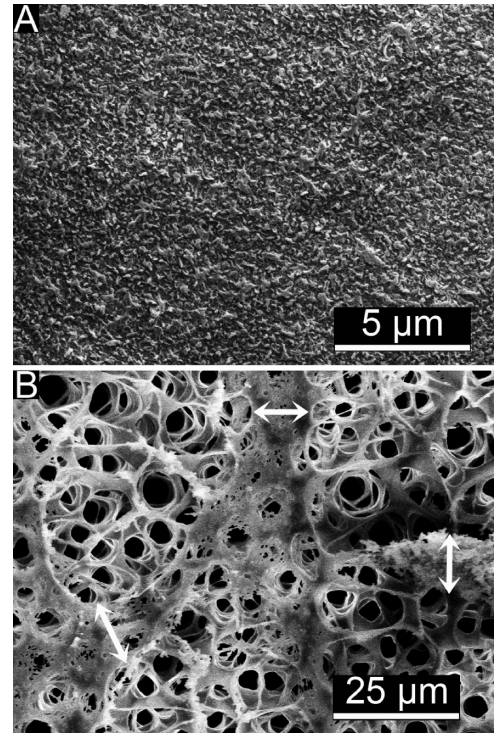

FIGURE 1. SEM micrographs displaying the structure of a TFC-FO membrane (TFC-FO-2) at the (a) top surface of the active polyamide layer and (b) at the bottom surface of the PSf support layer. The white arrows indicate the areas where the PET fibers and PSf layer were in contact, as evidenced by a visibly lower porosity.

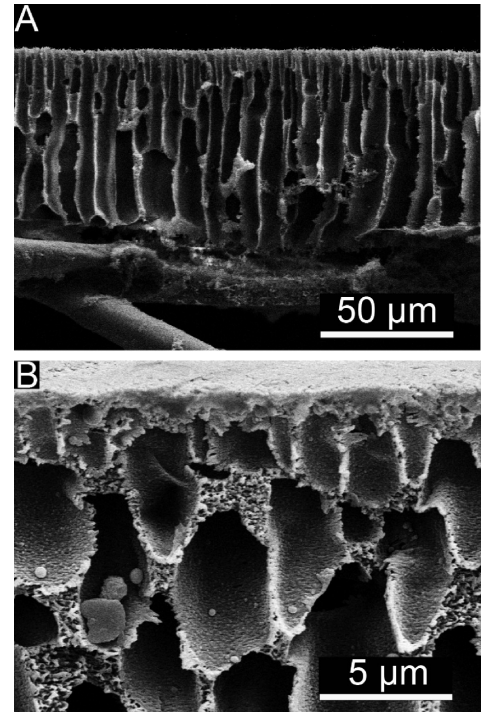

FIGURE 2. SEM micrographs of the cross-section of a TFC-FO membrane (TFC-FO-2) (a) including PET nonwoven fabric and (b) a magnified view of the dense, sponge-like morphology near the active layer. The average total membrane thickness is 95.9 $\pm$ 12.6 μm as determined using a digital micrometer.

solution to the nonsolvent bath. As a result of this exchange, the composition of the polymer film changes until the stability limit of the system is reached, where it phase separates into a polymer-rich and a polymer-poor phase. These two phases eventually form the polymer matrix and pores, respectively. The pore morphology is determined by the polymer precipitation rate—rapid precipitation produces finger-like pores and slow precipitation produces sponge-like pores (*11, 24*). When the in-flux of nonsolvent and the out-flux of solvent are nearly equal in magnitude, the net flux is small, and the polymer solution is slowly exposed to the nonsolvent. Slowly exposing the polymer to nonsolvents results in a slow precipitation rate, and sponge-like pores form. However, rapid precipitation occurs when the in-flux of nonsolvent dominates the net flux, producing finger-like pores.

NMP, the primary solvent used, permeates into the nonsolvent bath more slowly because it is a more favorable solvent for PSf, while the cosolvent DMF, a less favorable solvent for PSf (*25*), quickly permeates into the nonsolvent bath. This difference in exchange rates between NMP and DMF results in rapid and slow precipitation rates, respectively, when pure solvents are used. In the mixed solvent system, the precipitation rate can be tailored by controlling the relative amounts of the two solvents. The addition of DMF to the casting solution slows the permeation of solvent into the nonsolvent bath, promoting the formation of the dense sponge layer at the top surface. The NMP increases the precipitation rate, leading to the formation of the underlying finger-like structure (*26*).

The PSf support layer was cast from a 12 wt % polymer solution. This is lower than polymer concentrations used in the production of conventional TFC-RO membranes, which typically range between 15 and 25 wt % (*17, 20*). A lower concentration of polymer in the casting solution facilitates the formation of the finger-like structure and also yields higher porosity in the resultant PSf layer (*20*). The benefits of these structural features of the PSf layer for FO operations are discussed below.

Performance of TFC-FO Membrane. Intrinsic water permeability, A, and salt rejection, R, of the TFC-FO membrane were measured in an RO cross-flow cell. Our fabricated TFC-FO membrane had an A value of 1.16 ± 0.06 L m^{-2}h^{-1}atm^{-1} ($3.18 \pm 0.17 \times 10^{-12}$ m s^{-1}Pa^{-1}), comparable to the values measured for the commercial TFC-RO membrane with and without the PET nonwoven fabric, 1.30 ± 0.04 L m^{-2}h^{-1}atm^{-1} ($3.55 \pm 0.10 \times 10^{-12}$ m s^{-1}Pa^{-1}) and 1.60 ± 0.05 L m^{-2}h^{-1}atm^{-1} ($4.06 \pm 0.29 \times 10^{-12}$ m s^{-1}Pa^{-1}), respectively. These similar transport parameters are anticipated because both types of TFC membranes use the interfacial polymerization of polyamide to form the selective layer. The HTI-CTA membranes, alternatively, are asymmetric cellulose acetate-based membranes and have a lower A value of 0.36 ± 0.11 L m^{-2}h^{-1}atm^{-1} ($0.98 \pm 0.31 \times 10^{-12}$ m s^{-1}Pa^{-1}).

FO water fluxes measured using a DI feed solution and a 1.5 M NaCl draw solution are presented in Figure 3a for the various membranes. Water flux values for individual runs with each TFC-FO membrane are summarized in Table 1. Our hand-cast TFC-FO membranes exhibited the highest water flux (18.15 ± 0.96 L m^{-2}h^{-1}), nearly twice that achieved by the commercial HTI-CTA membranes (9.58 ± 0.11 L m^{-2}h^{-1}). As anticipated, the TFC-RO membranes with the PET fabric attached performed poorly in FO tests, yielding very low water fluxes (2.22 ± 0.22 L m^{-2}h^{-1}). However, after the PET fabric was removed, performance improved to 7.26 ± 0.87 L m^{-2}h^{-1}. Despite having a lower intrinsic water permeability, the better performance of the HTI-CTA membrane, over the TFC-RO membrane, highlights the paramount significance of the support layer structure in influencing FO water flux (*12*).

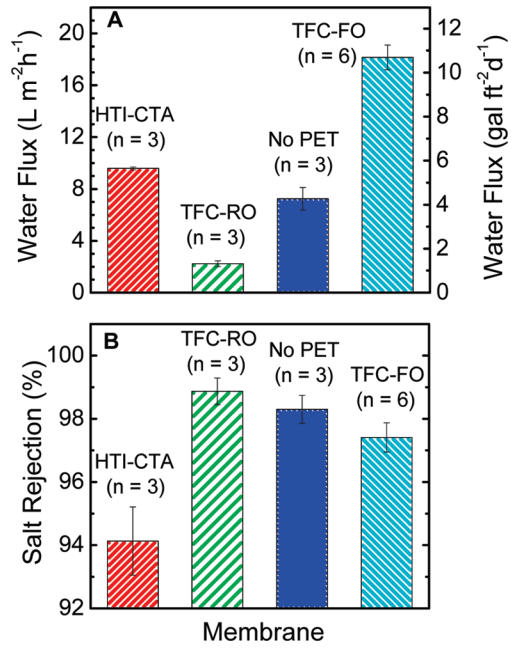

FIGURE 3. Comparison of (a) FO water flux and (b) salt rejection between TFC-FO membranes and commercial membranes: HTI-CTA (FO membrane), TFC-RO (RO membrane), and TFC-RO membrane after removal of the PET nonwoven fabric ("No PET"). The number of samples, *n*, used to obtain average and standard deviation is indicated. Experimental conditions for FO flux were as follows: 1.5 M NaCl draw solution, DI feed solution, and feed and draw solution temperature of 25 °C. Experimental conditions for salt rejection in RO measurement were as follows: 50 mM NaCl feed solution, 400 psi applied pressure, cross-flow of 21.4 cm/s, and temperature of 25 °C.

Figure 3b presents the observed salt rejection, R, using a 50 mM NaCl feed at a pressure drop of 400 psi (27.2 atm). The TFC membranes gave average salt rejections higher than those observed for the HTI-CTA membranes, which had an average R of 94.1 ± 1.1%. This observation is expected because thin-film composite membranes generally have higher salt rejection rates than asymmetric membranes (*27*). The TFC-RO membranes had average salt rejections of 98.9 ± 0.4 and 98.3 ± 0.4%, before and after the PET fabric had been removed, respectively. The similarity between salt rejections before and after fabric removal indicates that peeling off the fabric does not compromise the integrity of the selective skin layer. The TFC-FO membranes developed in this work have an average salt rejection of 97.4 ± 0.5%, slightly lower than the rejection observed for the commercial TFC-RO membranes. This difference is attributed to human variability, which occurs as a result of the hand-casting procedure. Characteristic performance values (e.g., A, B, J_w, and R) for the membranes used in this study are tabulated in Table 1 and in the Supporting Information (Tables S1 and S2).

TFC-FO Membrane Structural Parameters. Water flux versus osmotic pressure difference for one of our TFC-FO membranes (TFC-FO-2, Table 1) is presented in Figure 4. Ideally, the curve would be linear, but internal concentration polarization (ICP) causes a nonlinear dependence (*13*). Minimizing ICP is crucial to the design of a high performance FO membrane (*16*). As water permeates across the membrane, diluting the draw solution at the active surface of the membrane, diffusion works to restore the concentration to that of the bulk draw solution. When diffusion is not rapid enough to keep the solution well-mixed, the effective osmotic pressure, and thus, the water flux, is reduced. Therefore, decreasing ICP relies on reducing the resistance to solute diffusion in the porous support. The diffusion coefficient of

TABLE 1. Summary of Measured Water Flux, Salt Rejection, And Calculated Structural Parameter, *S*, for All The TFC-FO Membranes Tested[a]

membrane	feed concentration (M)	draw solute and concentration (M)	$\Delta\Pi^b$ (atm)	experimental FO Flux (L $m^{-2}h^{-1}$)	salt rejection (%)	structural parameter *S* (μm)
TFC-FO-1	DI	1.5 M NaCl	75.1	19.51	97.1	431
TFC-FO-2	DI	1.5 M NaCl	75.1	16.81	98.4	540
TFC-FO-3	DI	1.5 M NaCl	75.1	17.57	97.5	517
TFC-FO-4	DI	1.5 M NaCl	75.1	17.95	97.2	482
TFC-FO-5	DI	1.5 M NaCl	75.1	18.93	97.3	478
TFC-FO-6	DI	1.5 M NaCl	75.1	18.17	97.1	506
avg.				**18.16**	**97.41**	**492**
st. dev.				**0.96**	**0.46**	**38**
TFC-FO-2	DI	1.5 M NH_4HCO_3	56.3	16.55		
TFC-FO-2	DI	1.5 M NH_4HCO_3 (after 7 days)	56.3	16.28		

[a] The experimental conditions are stated. Temperature for all tests was 25 ± 0.5 °C. [b] Calculated by a software package from OLI Systems, Inc. (Morris Plains, NJ).

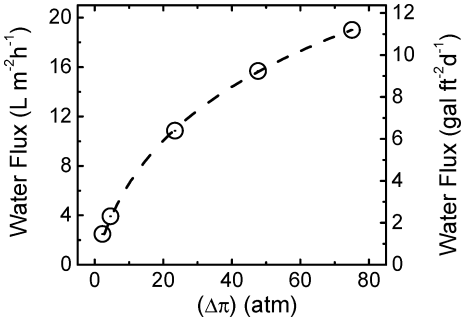

FIGURE 4. Experimental TFC-FO membrane water flux (open circles) over a range of osmotic pressure differences (i.e., draw solution osmotic pressure minus feed osmotic pressure) obtained using NaCl. The data points shown correspond to NaCl concentrations of 0.05, 0.1, 0.5, 1, and 1.5 M. Osmotic pressures were calculated from the corresponding salt concentrations using a software package from OLI Systems, Inc. (Morris Plains, NJ). Feed concentration is held constant (DI) while draw solution concentration is varied. Other experimental conditions were as follows: crossflow rate (feed and draw solution) of 21.4 cm/s and temperature of both feed and draw solutions of 25 °C. Data are fitted using eq 2 (dash line) to obtain value of the resistance to solute transfer, K.

the draw solute is fixed, leaving only the structural parameter *S* (defined earlier in eq 4) as a means to reduce ICP. *S* has units of length and can be thought of as the characteristic distance a solute particle must travel to reach the active layer of the membrane from the bulk draw solution. FO membranes with thinner, more porous, and less tortuous support layers will have smaller values of *S* and produce higher water fluxes.

The structural parameter *S* for our TFC-FO membrane (TFC-FO-2, Table 1) is determined by fitting the experimental data in Figure 4 to eq 2. The dashed line is the curve calculated using a value of 1.61×10^{-9} m^2/s for D_{NaCl} (*28*) and 442 μm for *S*. We also use eq 2 to find *S* for the individual FO membranes using the corresponding measured water flux data (Table 1). The average value obtained from these runs, 492 ± 38 μm, agrees well with the data, fitting over a range of draw solution concentrations as shown in Figure 4. Our calculations also give *S* values of 595 ± 114 μm for the HTI-CTA membranes, and 9583 ± 1351 μm and 2155 ± 292 μm for the TFC-RO membranes with and without the PET fabric, respectively. Individual values of *S* for the various membranes tested are tabulated in Table S3 of the Supporting Information.

Comparing cross-sectional SEM micrographs of the commercial membranes in Figure 5 with those taken of our TFC-FO membranes (Figure 2) demonstrates the link between membrane structure and the structural parameter *S*. Figure

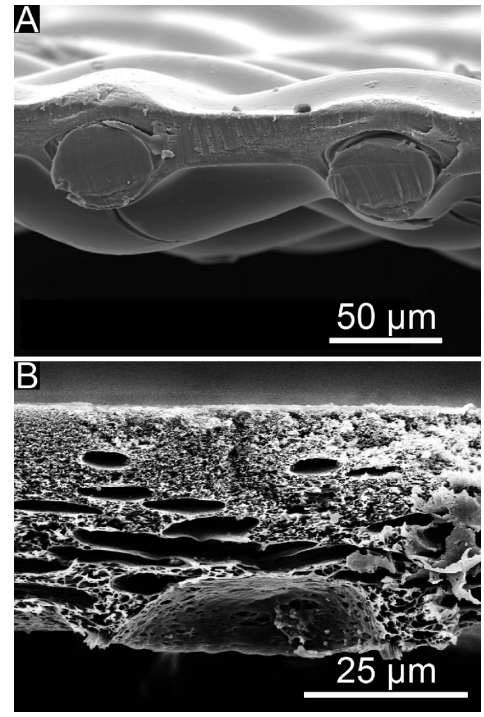

FIGURE 5. SEM micrographs display the cross-section of (a) commercial HTI-CTA membrane and (b) TFC-RO membrane after removing the PET nonwoven fabric. Thickness of the asymmetric membrane was approximately 95 μm; the TFC-RO membrane was approximately 125 and 50 μm, before and after PET removal, respectively, as confirmed using a digital micrometer.

5a presents the unique structure of the HTI-CTA cross-section. The SEM micrograph shows what appears to be a woven mesh embedded in a continuous polymer layer. The overall thickness is ~100 μm, as confirmed with a micrometer (94.4 ± 0.3 μm). By embedding the woven mesh within the continuous polymer layer, the need for a thick backing layer is eliminated. However, the membrane appears denser than our TFC-FO membrane, thereby explaining its inferior performance.

The TFC-RO membrane consists of a thin active layer supported by a microporous polymer layer, which is backed by a nonwoven fabric (Figures 5b and S4 of the Supporting Information). Estimates from micrographs give a microporous polymer support thickness of ~50 μm and a nonwoven backing fabric thickness of 75 μm. These values are consistent with measurements made using a micrometer: 125.1 ± 0.7 μm for the entire membrane and 50.6 ± 2.8 μm

for the membrane after removing the nonwoven fabric layer. The support layer of the membrane appears to have a sponge-like morphology, which is necessary for RO operations because the finger-like structures or macrovoids can compromise the mechanical integrity (*26*). However, unlike RO, FO does not require applied hydraulic pressure, and the higher resistance to mass transfer of the sponge-like microstructure compared to the finger-like microstructure is a hindrance. The significant resistance to mass transfer of the sponge-like morphology is evidenced by the higher calculated S value (2155 ± 292 μm, Table S3 of the Supporting Information) for the relatively thin (50 μm) TFC-RO membrane without PET.

Membrane Performance and Chemical Stability with Ammonium Bicarbonate Draw Solution. The HTI-CTA membrane is cellulose-based, precluding its use with the ammonia-carbon dioxide draw solution. Cellulose acetate degrades at exponentially increasing rates when operated outside its stable pH range of 4−6 (*11, 29*), while our TFC-FO membrane should be stable up to pH 11 because it uses a polyamide chemistry (*30*). We have tested the chemical stability of the TFC-FO membrane by measuring the water flux using a 1.5 M NH_4HCO_3 draw solution (pH 7.9). The observed water flux of 16.55 L $m^{-2}h^{-1}$ agrees well with the water flux predicted for an osmotic pressure of 827 psi (56.3 atm) generated by the 1.5 M NH_4HCO_3 draw solution. After this initial test, the membrane was soaked in the 1.5 M ammonium bicarbonate solution for 7 days. Following this exposure, no visual changes were observed and the water flux remained constant (16.28 L $m^{-2}h^{-1}$) demonstrating the chemical stability of our membrane.

Implications for FO Membrane Development. The membranes developed in this work demonstrate the fabrication of a TFC-FO membrane that is chemically stable and is less hindered by internal concentration polarization. Further improvements to TFC-FO membrane performance are possible through tailoring the support membrane structure (*31*), modifying the support membrane chemistry (*12*), and optimizing the interfacial polymerization conditions (*27*). The membrane structural parameter S shows that by increasing the void fraction and decreasing the thickness and tortuosity, the resistance to mass transfer can be reduced. Decreasing the membrane thickness to 40 μm, a goal that can be achieved using industrial coating equipment, would improve the structural parameter from 492 to 205 μm. Varying the casting conditions can further optimize the microporous support structure (*11, 20*), decreasing the structural parameter and thereby improving TFC-FO membrane performance. New, more hydrophilic chemistries obtained using a different polymer (e.g., polyethersulfone) or the addition of hydrophilic additives (e.g., polyethylene oxide or poly(4-vinylpyrilidine)) may also improve FO membrane performance as previous research suggests (*12*). Finally, several different interfacial polymerization chemistries have been used to make membranes. Polyamides remain the standard for desalination, but different chemistries might be well-suited for other osmotically driven membrane processes (*27*). These new TFC-FO membranes may find application in a variety of processes, such as seawater and brackish water desalination, wastewater reclamation and reuse, and energy generation by pressure retarded osmosis (*32*).

Acknowledgments

The work was supported by a Graduate Fellowship (to N.Y.Y.) made by the Environment and Water Industrial Development Council of Singapore; the WaterCAMPWS, a Science and Technology Center of Advanced Materials for the Purification of Water with Systems under the National Science Foundation Grant No. CTS-0120978; Oasys Water Inc.; and the KAUST-Cornell Center for Energy and Sustainability. We thank Eric Hoek and his research group at UCLA for useful guidance on protocols for interfacial polymerization.

Supporting Information Available

Additional SEM micrographs of the polyamide active layer surface of the forward osmosis TFC membrane (Figure S1); additional SEM micrographs of polysulfone support bottom surface of the forward osmosis TFC membrane (Figure S2); additional SEM micrographs of cross-section of the forward osmosis TFC membrane (Figure S3); SEM micrograph displaying the cross-section of a TFC-RO membrane before removing the PET nonwoven fabric (Figure S4); intrinsic permeability, salt permeability coefficient, and salt rejection for the RO runs (Table S1); FO water flux and performance ratio for all the forward osmosis runs carried out in this study under the stated conditions (Table S2); summary of structural parameters of the membranes used in this study (Table S3).This material is available free of charge via the Internet at http://pubs.acs.org.

Literature Cited

(1) Kravath, R. E.; Davis, J. A. Desalination of sea-water by direct osmosis. *Desalination* **1975**, *16* (2), 151–155.
(2) Cath, T. Y.; Childress, A. E.; Elimelech, M. Forward osmosis: Principles, applications, and recent developments. *J. Membr. Sci.* **2006**, *281* (1−2), 70–87.
(3) Cath, T. Y.; Gormly, S.; Beaudry, E. G.; Flynn, M. T.; Adams, V. D.; Childress, A. E. Membrane contactor processes for wastewater reclamation in space Part I. Direct osmotic concentration as pretreatment for reverse osmosis. *J. Membr. Sci.* **2005**, *257* (1−2), 85–98.
(4) Cartinella, J. L.; Cath, T. Y.; Flynn, M. T.; Miller, G. C.; Hunter, K. W.; Childress, A. E. Removal of natural steroid hormones from wastewater using membrane contactor processes. *Environ. Sci. Technol.* **2006**, *40* (23), 7381–7386.
(5) Cath, T. Y.; Adams, D.; Childress, A. E. Membrane contactor processes for wastewater reclamation in space II. Combined direct osmosis, osmotic distillation, and membrane distillation for treatment of metabolic wastewater. *J. Membr. Sci.* **2005**, *257* (1−2), 111–119.
(6) Holloway, R. W.; Childress, A. E.; Dennett, K. E.; Cath, T. Y. Forward osmosis for concentration of anaerobic digester centrate. *Water Res.* **2007**, *41* (17), 4005–4014.
(7) Achilli, A.; Cath, T. Y.; Marchand, E. A.; Childress, A. E. The forward osmosis membrane bioreactor: A low fouling alternative to MBR processes. *Desalination* **2009**, *239* (1−3), 10–21.
(8) Jiao, B.; Cassano, A.; Drioli, E. Recent advances on membrane processes for the concentration of fruit juices: a review. *J. Food Eng.* **2004**, *63* (3), 303–324.
(9) Garcia-Castello, E. M.; McCutcheon, J. R.; Elimelech, M. Performance evaluation of sucrose concentration using forward osmosis. *J. Membr. Sci.* **2009**, *338* (1−2), 61–66.
(10) McCutcheon, J. R.; McGinnis, R. L.; Elimelech, M. A. novel ammonia-carbon dioxide forward (direct) osmosis desalination process. *Desalination* **2005**, *174* (1), 1–11.
(11) Baker, R., *Membrane Technology and Applications*, 2nd ed.; Wiley: New York, 2004; p 552.
(12) McCutcheon, J. R.; Elimelech, M. Influence of membrane support layer hydrophobicity on water flux in osmotically driven membrane processes. *J. Membr. Sci.* **2008**, *318* (1−2), 458–466.
(13) McCutcheon, J. R.; Elimelech, M. Influence of concentrative and dilutive internal concentration polarization on flux behavior in forward osmosis. *J. Membr. Sci.* **2006**, *284* (1−2), 237–247.
(14) Lee, K. L.; Baker, R. W.; Lonsdale, H. K. Membranes for power-generation by pressure-retarded osmosis. *J. Membr. Sci.* **1981**, *8* (2), 141–171.
(15) Loeb, S.; Titelman, L.; Korngold, E.; Freiman, J. Effect of porous support fabric on osmosis through a Loeb-Sourirajan-type asymmetric membrane. *J. Membr. Sci.* **1997**, *129* (2), 243–249.
(16) McCutcheon, J. R.; Elimelech, M. Modeling water flux in forward osmosis: Implications for improved membrane design. *AIChE J.* **2007**, *53* (7), 1736–1744.
(17) Cadotte, J. E. Interfacially synthesized reverse osmosis membrane. 4277344, 1981.
(18) McCutcheon, J. R.; McGinnis, R. L.; Elimelech, M. Desalination by ammonia-carbon dioxide forward osmosis: Influence of draw and feed solution concentrations on process performance. *J. Membr. Sci.* **2006**, *278* (1−2), 114–123.

(19) Ang, W. S.; Elimelech, M. Protein (BSA) fouling of reverse osmosis membranes: Implications for wastewater reclamation. *J. Membr. Sci.* **2007**, *296* (1−2), 83–92.
(20) Mulder, J. *Basic Principles of Membrane Technology*, 2nd ed.; Springer: New York, 1996; p 584.
(21) Hoek, E. M. V.; Kim, A. S.; Elimelech, M. Influence of crossflow membrane filter geometry and shear rate on colloidal fouling in reverse osmosis and nanofiltration separations. *Environ. Eng. Sci.* **2002**, *19* (6), 357–372.
(22) Ghosh, A. K.; Jeong, B. H.; Huang, X. F.; Hoek, E. M. V. Impacts of reaction and curing conditions on polyamide composite reverse osmosis membrane properties. *J. Membr. Sci.* **2008**, *311* (1−2), 34–45.
(23) Cadotte, J. E.; K, R. S.; Sand, J. E.; Petersen, R. J. Improved Porous Supports for Thin-Film Composite Reverse Osmosis Membranes. *Report for Office of Water Research and Technology* **1981**, 51 p.
(24) Strathmann, H.; Kock, K.; Amar, P.; Baker, R. W. Formation mechanism of asymmetric membranes. *Desalination* **1975**, *16* (2), 179–203.
(25) Hansen, C. M. *Hansen Solubility Parameters: A User's Handbook*, 2nd ed.; CRC Press: Boca Raton, 2007; p 519 p.
(26) vandeWitte, P.; Dijkstra, P. J.; vandenBerg, J. W. A.; Feijen, J. Phase separation processes in polymer solutions in relation to membrane formation. *J. Membr. Sci.* **1996**, *117* (1−2), 1–31.
(27) Petersen, R. J. Composite reverse-osmosis and nanofiltration membranes. *J. Membr. Sci.* **1993**, *83* (1), 81–150.
(28) Lobo, V. M. M. Mutual diffusion-coefficients in aqueous-electrolyte solutions (technical report). *Pure Appl. Chem.* **1993**, *65* (12), 2614–2640.
(29) Vos, K. D.; Burris, F. O.; Riley, R. L. Kinetic study of hydrolysis of cellulose acetate in pH range of 2−10. *J. Appl. Polym. Sci.* **1966**, *10* (5), 825–832.
(30) Cadotte, J. E.; Petersen, R. J.; Larson, R. E.; Erickson, E. E. New thin-film composite seawater reverse-osmosis membrane. *Desalination* **1980**, *32* (1−3), 25–31.
(31) Ghosh, A. K.; Hoek, E. M. V. Impacts of support membrane structure and chemistry on polyamide−polysulfone interfacial composite membranes. *J. Membr. Sci.* **2009**, *336* (1−2), 140–148.
(32) McGinnis, R. L.; Elimelech, M. Global challenges in energy and water supply: The promise of engineered osmosis. *Environ. Sci. Technol.* **2008**, *42* (23), 8625–8629.

ES1002555